Combined energy – diffraction data refinement of decagonal AlNiCo

M. Mihalkovič[1,3], C. L. Henley[2] and M. Widom[1]

[1] *Physics Dept., Wean Hall, Carnegie-Mellon University, Pittsburgh PA 15213 USA*
[2] *Physics Dept., Clark Hall, Cornell University, Ithaca NY 14853 USA*
[3] *Institute of Physics, Slovak Academy of Sciences, Bratislava, Slovakia*

Abstract

We incorporate realistic pair potential energies directly into a non-linear least-square fit of diffraction data to quantitatively compare structure models with experiment for the Ni-rich d(AlNiCo) quasicrystal. The initial structure models are derived from a few *a priori* assumptions (gross features of the Patterson function) and the pair potentials. In place of the common hyperspace approach to the structure refinement of quasicrystals, we use a real-space tile decoration scheme, which does not rely on strict quasiperiodicity, and makes it easy to enforce sensible local arrangements of the atoms. Inclusion of the energies protects the fit procedure from converging on spurious solutions. The method pinpoints sites which are likely to break the symmetry of their local environment.

Keywords: quasicrystals; structure refinement; d-AlNiCo

1. Introduction

Recently, two high-quality refinements have been published from single-crystal X-ray data from the "basic Ni-rich" phase of d(AlNiCo) [3, 4]. At the same time, a Monte Carlo method was developed [6] to *predict* the same structure, approximating the Hamiltonian with pair potentials, and using as inputs only the crystallographic parameters (plus the fact that the structure is strongly layered). Here, we present the first trial of a combined method which uses energy and diffraction information to fix complementary features of the atomic structure.

The decagonal AlNiCo system exhibits a variety of metastable and stable phases, out of which the "basic Ni-rich" phase [2] has attracted many detailed studies due to its high structural quality. The refined structures of [3] and [4] agree on basic features, but they differ in many important details. The refinement presented by CHS [3] exhibits 8Å periodicity along the vertical axis, lacks 10-fold screw symmetry property, and does not lend itself an easy interpretation in terms of a tiling geometry. The structure solution of [4] has 4Å periodicity, and can be readily interpreted in terms of the Hexagon-Boat-Star (HBS) tiling with edge length of ∼6.5Å tiling geometry. The R-factors achieved are comparable in the two cases.

Quasicrystals, as aperiodic structures, typically include local patterns which are rare enough to be ill-determined from diffraction, but common enough to have a significant effect on physical properties (such as total energy or conductivity). Thus the problem of structure prediction from energies becomes entangled with structure fitting from diffraction: we suspect that, in the future, the best quasicrystal structure fits will combine the two inputs in some fashion.

Here, we present the first structure fit in quasicrystals, in which energy and diffraction information are combined in the same objective function. Previously, powder diffraction data on i-TiZnNi [5] was systematically refined with energy inputs. In that work, each type of information was used separately to fix the degrees of freedom which are most sensitive to it: a least-squares refinement from that data determined the species occupying each site type, and this was alternated with ab-initio calculations to relax the positions.

In the present study we calculate energetics from pair potentials microscopically derived using "generalized pseudopotential theory" (GPT) by Moriarty and Widom [8], a total of six functions (e.g. $V_{\mathrm{AlNi}}(r)$) for all combinations of the species. The prominent

feature of these potentials is Friedel oscillations, so that a typical potential has three minima before the cutoff radius (which we chose to be 10 Å). The atom sites are called $\{\vec{\mathrm{R}}\}$, with $\chi(\vec{\mathrm{R}})$ designating the chemistry (Al, Ni, or Co) of that site. A convenient diagnostic tool in the refinement of a decoration structure [9] is the "site energy", the portion of total energy ascribed to interactions of site $\vec{\mathrm{R}}$:

$$E^{\mathrm{site}}(\vec{\mathrm{R}}) \equiv \sum_{\vec{\mathrm{R}}'} V_{\chi(\vec{\mathrm{R}})\chi(\vec{\mathrm{R}}')}(|\vec{\mathrm{R}} - \vec{\mathrm{R}}'|). \qquad (1)$$

Then the total energy is

$$E_{\mathrm{tot}} \equiv \frac{1}{2} \sum_{\vec{\mathrm{R}}\vec{\mathrm{R}}'} E^{\mathrm{site}}(\vec{\mathrm{R}}). \qquad (2)$$

Whereas previous refinements of quasicrystals have used the hyperspace-cut representation of the structure, our results demonstrate the equal effectiveness of an alternative approach, the tile-decoration framework. The value of the tiling-decoration approach is that the structure models do not rely on periodicity or quasiperiodicity, and they are naturally represented in "real" space. Consequently, decoration is an elegant way [5] to transfer/combine information between the different system sizes appropriate for different calculations, *e.g.*: (i) numerical diffraction calculations from a large approximant; (ii) eventual Monte Carlo simulations using a tile reshuffling update and a tile-tile Hamiltonian, in a smaller approximant; (iii) molecular dynamics using pair potentials; (iv) atom relaxation using an ab-initio total energy code, which is typically feasible only in the smallest approximants.

The decoration formulation might be attractive for dealing with *randomness* (an issue we ignored in the present contribution, however). A realistic structure model is an *ensemble* of atomic configurations. When the contents of different sites are independent random variables, then a stochastic, mixed occupation of each site is a fair description. If, however, the sites are highly correlated, a random tiling may be a more reasonable model; indeed, that is our present picture of the "basic Ni" phase of *d*-AlNiCo [6], in contrast to *d*-AlCuCo, with indications of obeying matching rules [15]. A tile-decoration is superior to a hyperspace description in the random-tiling case: all the randomness may be ascribed to the tile configurations, while the decoration of each tiling is deterministic. Some of the technical questions of a random-tiling structure refinement were discussed in Sec.5 of Ref. [10].

2. Structure modeling for combined fit

To explain the decoration approach, we review nomenclature introduced in [9]: A *decoration* is a mapping which, given any valid tile-configuration, produces a set of atom sites. The sites are grouped into *orbits*, each of which is *bound* to a particular kind of tile, and lies in the same positions on every tile of that kind (An orbit plays a role like an orbit of symmetry-related Wyckoff positions in a crystal structure. In the hyperspace-cut representation of a quasiperiodic structure, each member of the decoration orbit on a representative tile would correspond to one subdomain of the acceptance domain in perpendicular space.).

More generally, orbits are bound to *tiling objects* which may be not only tiles, but other geometrical constituents of the tiling such as tile vertices – e.g. we may choose to surround every vertex by an identical symmetric cluster. Another kind of a tiling object is defined to overlay a certain local pattern in the tiling. We can then introduce context dependence by *rebinding* certain atoms to the new tiling object. Other atoms remain bound to the old objects, so we do not define too many positional parameters. One decoration rule is a *rebinding* of another if it has more orbits, and the family of structures produced from the original decoration (by varying the parameter values) is a subset of the family produced from the rebinding decoration.

By default we require that atomic decorations inherit the symmetry of the tiling objects so that placing an atom at general position will generate all symmetry equivalent sites. Furthermore, preservation of the site symmetry constrains the degrees of freedom for atomic displacements. In reality, forcing atomic motifs to obey the point symmetry of tiling object is not always energetically favourable.

In the tile-decoration machinery, such situations are handled by the concept of *symmetry-breaking*: a *flavour* (like an arrow on a tile) is associated with each (broken) symmetry related variant. [9], so that the decoration remains formally deterministic and reflects the symmetries of the flavoured tiles. The flavours may be initialized randomly, and in the simulation process (for example Monte Carlo annealing) the symmetry-breaking may be effectively used as an update move.

The decoration rule for our combined fit is adapted from the deterministic model of [6], in which atoms decorate an HBS tiling with edge length a_q ∼6.4Å. (similar to Fig. 3a of [6], but without the complication of the "bow-tie" defects shown there.)

This model was derived by successive elimination of the degrees of freedom in Monte-Carlo simulations with the GPT pair potentials. Throughout the paper we use a simple convention, with HBS edge vectors are $a_q\vec{e}_i$, where $\vec{e}_i \equiv (\cos(2\pi i/5), \sin(2\pi i/5))$. Notice that our Hexagon tile has a mirror plane running down its long axis, but not transverse: we should visualize it as if marked by an arrow to distinguish the

two ends. In the same way, the Boat's mirror symmetry and the Star tile's fivefold rotation symmetry are broken to allow for our decoration.

Our "basic" rule uses as supplementary tiling objects the Fat rhombi (which appear naturally when the HBS tiles are subdivided into Penrose rhombi), as well as the interior vertices thereby created; this captures the similarity of the local environments in all the 72° corners of HBS tiles. This rule is shown in Fig.1. All Ni atoms are ascribed to the HBS edges, Co atoms decorate the supplementary interior vertices , as well as a site on the long diagonal of every Fat rhombus. Orbits 12 and 16 implement the broken symmetries of the Boat and Star. In the end, this decoration rule associates 16 orbits with nine tiling objects, and yields 38 positional parameters.

Refinement using the "basic" binding motivated a more complex "augmented" binding (Table 1), that proved to be more successful in fitting the data. Firstly, since the Ni(3) orbit alone contains more than 20% of all atoms, we split it among 3 objects, "context-sensitive" HBS Nodes. In both approximants we used, three classes of HBS vertex stars occure: 5-fold, 3-fold and 2-fold (in random HBS, also 4-fold and another 3-fold vertex type occurs). The symmetry of these objects gives rise to 4 Ni orbits, labelled Ni(3_a-3_d). The new orbits are listed in Table 1 below the horizontal line. Second, one of the two Al(15) atoms has been replaced by vacancy implementing symmetry-breaking of the Hexagon mirror (Al(15+) in the Table 1), and new atom Al(17) has been placed near the center of the Hexagon.

The atomic density for the decoration rule (in either binding variant) is 0.0705 atoms/Å^3, and the composition is $Al_{70}Ni_{20.7}Co_{9.3}$, slightly richer in Co than the CHS sample ($Al_{70.6}Ni_{22.7}Co_{6.7}$). When the atoms are fixed at "ideal" sites, the minimal distance occuring between Al-Al, Al-Co and Al-Ni pairs is 2.46Å. The structural energy of this initial model is -0.297 eV/atom for a small approximant with 214 atoms per unit cell; using positional degrees of freedom of the decoration rule it relaxes to -0.393 eV/atom. Fully relaxed energy (atomic displacements for atoms in the same orbit no longer equivalent) is -0.422 eV/atom, and finally allowing atoms to relax their positions in double period (8Å) unit cell, energy drops to -0.442 eV/atom.

Periodic approximants. A drawback of the tile-decoration approach is that the infinite non-periodic quasicrystal must usually be handled indirectly, being approximated by an periodic "approximant". This necessarily has a "background phason strain" which is, roughly, the average tilt of the cut through hyperspace away from the irrational orientation with 10-fold symmetry.) Consequently, each orbit of reciprocal lattice vectors $\vec{Q}$ of the quasicrystal gets split into several inequivalent orbits of the approximant's reciprocal lattice vectors $\vec{Q}_{\rm app}$. In the fit, we selected only one representative $\vec{Q}_{\rm app}$ for each decagonal $\vec{Q}$, since the number of datapoints is already large, but we monitored systematically the errors thus introduced, calculating $\sigma_{\rm app}$ as the r.m.s. deviation of the difraction amplitudes among all $\vec{Q}_{\rm app}$ mapping on a given $\vec{Q}$. For the larger approximant discussed below, $\sigma_{\rm app}$ was similar to or less than the experimentally observed uncertainty for all peaks.

A more systematic treatment of the approximant diffraction amplitudes would be to symmetrize over all those deriving from a single orbit of quasicrystal $\vec{Q}$. This would demand careful handling of the phase factors, by properly centering the approximant structure both in real and in perpendicular space [5].

A further difficulty is that for smaller approximants, different quasiperiodic $\vec{Q}$ vectors may map on the same approximant $\vec{Q}_{\rm app}$. We found the smallest orthorhombic approximant avoiding such ambiguous mappings for *all* reflections in the CHS data set has edge lengths 61Å × 32Å in the decagonal plane. In the following, we label this approximant T_{42} (for the number of HBS vertices per unit cell). For our decoration rule it contains 560 atoms per unit cell. We found it satisfactory to use just one more bigger approximant, with both sides in the decagonal plane larger by a factor of $\tau \equiv (\sqrt{5}+1)/2$. We denote this tiling T_{110}.

3. Procedure

Dataset. We used the CHS dataset [3] . It dataset contains 2767 unique reflections under the assumption of $10/m$ Laue group; by averaging over symmetry-related amplitudes, to enforce $10/mmm$ Laue symmetry, a set with 1544 unique reflections is obtained. The two possibilities gave about equal internal R-factors. Our structure model has $P10_5/mmc$ space group, so we used the smaller $10/mmm$ data set. (Using the $10/m$ set gave practically the same results, except that typically both the R_w and R factor are increased by 1%.)

The partial diffraction amplitude for tiling orbit j is

$$F_j^{\rm orb}(\vec{Q}) = \sum_\alpha W_{j\alpha}(\vec{Q}) f_\alpha(\vec{Q}) \sum_{\vec{R}\in j:\chi(\vec{R})=\alpha} e^{i\vec{Q}\cdot\vec{R}}. \quad (3)$$

The inner summation in (3) runs over all atoms of species α in orbit j, and $f_\alpha(\vec{Q})$ is the atomic form factor for that species. The Debye-Waller (DW) coefficients ${b^{xy}}_{j,\alpha}$ and ${b^z}_{j,\alpha}$ couple with decagonal-plane and vertical $\vec{Q}$ components, and take different values not only for different orbits, but also for different

species occupying the same orbit:

$$W_{j\alpha}(\vec{\mathrm{Q}}) = \exp[-\frac{1}{4}(b^{xy}{}_{j\alpha}\vec{\mathrm{Q}}^2_{xy} + b^{z}{}_{j\alpha}\vec{\mathrm{Q}}^2_{z}] \qquad (4)$$

The total calculated diffraction amplitude is then

$$F^{calc}(\vec{\mathrm{Q}}) = e^{-\frac{1}{4}b_\perp \vec{\mathrm{Q}}^2_\perp} |\sum_j F^{\mathrm{orb}}{}_j(\vec{\mathrm{Q}}). \qquad (5)$$

where we introduced a single perp-space DW coefficient $b_\perp$. Finally, we compute goodness/reliability factors

$$\chi^2 \equiv \sum_{\vec{\mathrm{Q}}} (F^{obs}(\vec{\mathrm{Q}}) - F^{calc}(\vec{\mathrm{Q}}))^2/\sigma(\vec{\mathrm{Q}})^2 \qquad (6)$$

$$R \equiv \sum_{\vec{\mathrm{Q}}} \frac{\big|F^{obs}(\vec{\mathrm{Q}}) - |F^{calc}(\vec{\mathrm{Q}})|\big|}{\sum_{\vec{\mathrm{Q}}} F^{obs}(\vec{\mathrm{Q}})}. \qquad (7)$$

As usual, the weighted R-factor, called R_w, is defined like (7) except that each term in the numerator and denominator acquires a factor $1/\sigma(\vec{\mathrm{Q}})^2$.

Implementation. We couple pair-potential energy with χ^2 via parameter λ in the objective function for the non-linear least-squares minimization:

$$U = \chi^2 + (E - E^{\mathrm{targ}})^2/\lambda^2 \qquad (8)$$

where E is the energy (2), per atom. Here E^{targ} is a "target" energy, [1] and is treated in the fit as a dummy datapoint with an "error bar" λ. E^{targ} may be set to the total structural energy per atom after an (unconstrained) relaxation $E^{\mathrm{un}}_{\mathrm{rel}}$.

Our fitting form (Eq. (4)) allows independent DW parameters b^{xy} and b^z for each orbit/species combination, but these are underdetermined by the data; to obtain sensible results, the fit needs to be biased towards having similar DW factors for similar atoms, in the spirit of the maximum-entropy method. We implement this by adding terms for b^{xy} and b^z to the χ^2 sum: before each iteration, we calculate the average DW factor for each species and the xy and z components of DW factor, and set them as datapoints for the next iteration, with appropriately chosen σ_{DW}.

4. Results

Fitting the "basic" binding to the CHS dataset we obtained reasonable, but not satisfactory R-factors R_w=0.122 and R=0.202. The large displacement of atom Al(15) (see Fig. 2, top) and other considerations motivated our "augmented" binding; Table 5summarizes our results for the latter. The symmetry-constrained relaxed energy E_{rel} of the @@ "augmented" rule is tolerably higher than E_{rel} of the "basic" rule (see Table 5). However, the combined fit improved dramatically, displacing the Al(15_a) atom towards the long body diagonal of H tile. We have selected two structure solutions by the combined fit, one with lowest R_w factor but rather high energy, and one with slightly worse R_w factor, but comparable in energy with the basic decoration rule (Table 5). @@ The $F_{calc}(\vec{\mathrm{Q}})$ from our fit is compared to the $F_{obs}(\vec{\mathrm{Q}})$ from the diffraction data in Fig. 3.

The fitted DW factors, especially those of Al, exhibit high degree of anisotropy. (Table 5.). This agrees with the TYT refinement [4] of a different sample of AlNiCo. (The TYT sample was slightly richer in Al and Co than the sample for the CHS data [3] that we are fitting here.)

Most of the TYT hyperatom orbits correspond to our HBS tile decoration orbits, and their individual orbit DW factors are mostly consistent with ours for the corresponding atoms. The most pronounced disagreement is just the orbit Al(15+) for which $b_z/b^{xy} \approx 5$ in our refinement, but $\approx 1/5$ in the TYT refinement (see Table 2 in Ref. [4], site label 9). This atom is at the same time displaced farthest from its ideal position for both TYT and our refinements, and the displacements have similar magnitude and direction for TYT and our "*basic*" binding (see Fig.2). In the "augmented" binding, Al(15+) occurs in a completely different environment, displacing towards long diagonal of H tile, which explains the discrepancy in the DW factors.

The TYT model and our decoration (in either variant) differ from the CHS model in having a larger space group symmetry (10-fold screw axis vs. a 5-fold axis, 4Å translation vs. 8Å translation), but also in other respects: higher atomic density, and absence of transition metals (TM) in the sites corresponding to hyperatom "B" in Ref. [3]. Our decorations are more constrained than the other models, in that @@ mixed Al-TM occupancy is disallowed, partial occupation appears only through symmetry-breaking, and unphysical close pairs never appear on account of the energy term in Eq.(8) The CHS model achieved a lower weighted R-factor (∼0.06) than the present refinement of the same data set, at the price of including many more parameters. It remains to be resolved whether the CHS model is the essentially unique minimum for their data set.

5. Discussion

The rearrangement of the atomic decoration inside the Hexagon tile – @@driven, we think, by the diffraction term in (8) – is reminiscent of the atomic shifts observed in molecular dynamics (MD) simulations under the same potentials with an initial atomic

[1] When $\Delta E \equiv E^{\mathrm{tot}} - E^{\mathrm{targ}} \gg \lambda$, as is usually the case in the orbit-constrained relaxation, then $U = \chi^2 + 2(\Delta E/\lambda^2)E^{\mathrm{tot}}$ would be practically equivalent to (8); since the likelihood of parameters is supposed to behave as $\exp(-U)$, $\lambda^2/2\Delta E$ is evidently playing the role of a temperature.

configuration similar to the present model [7]. In those simulations, using supercells 8Å or 16Å thick in the stacking direction, slow cooling led to a more favourable arrangement of atoms, in which one Al was pushed from the Al(15) position towards the center of the Hexagon, while the other moved @@ onto the long body diagonal of the Hexagon. However, in contrast to our present model in which two such atoms get squeezed into a column, in [7] only one atom per 8Å period was displaced in this fashion, so that the column in the Hexagon center contained three Al atoms per 8Å period. A recent MD study [11] confirms that the optimal Hexagon decoration has 8Å period, with atomic arrangement topologically equivalent to the result of our combined fit, but in [11] the atomic sites in the second 4Å bilayer are *flipped* in each Hexagon across a mirror plane perpendicular to its body diagonal. @@ These findings again call for study of the so-called "stacking–fault" mechanism, in which the decoration rule would – at least in a zero-order approximation – remain essentially a 4Å rule, and the variations in the decoration from one 4Å bilayer to the next would be described by "flips" of the tiles, occuring independently in each bilayer.

@@ The discussed variations in the atomic structure also illuminate a motif generally considered important in decagonal structures: the 20Å diameter decagon. One such cluster in marked in Fig. 2 by the inscribed dashed circle. near the inner ring of 10 TM and . Note the inner ring containing ∼20 Al atoms (Al(17) and Al(9))"squeezed" in between 10 TM atoms (typically Co, sometimes Ni), a feature that emerges in many HREM/HAADF images [1, 12]. This could appear as an optimal configuration in a 4Å bilayer *only* when energy and diffraction data are combined. On the other hand, as suggested by the MD studies, it *should* emerge as a low energy configuration from simulations performed for stacked bilayers.

In conclusion, we used tile-decoration machinery to set up a combined energy–diffraction data fit of the d-AlNiCo structure. The resulting R-factors are comparable to those from a previous study [3], while using fewer parameters, and not allowing ad-hoc averaged/mixed site occupancies. Apart from the implementation of energies into the diffraction fit, at this stage our refinement is completely analogous to the hyperspace refinements, since we used strictly approximants of the ideal, unperturbed quasiperiodic tiling. The possible disorder correlations hidden in the experimental data are still lumped into global parameters of the fit, mainly the perp-space DW factor.

Clearly, the future prospect is to take full advantage of the real-space formulation of the problem and recover the correlations in atomic occupancies directly from the "grand combined fit". This would use Monte Carlo annealing to sample all relevant degrees of freedom (swapping individual atoms, flipping symmetry-broken tiling objects) in conjunction with optimizing R-factors fitting the diffraction data. [10] If the "realistic" pair potentials prove indeed sufficiently realistic, the fit parameters may be further constrained by DW factors pre-calculated from zero-T phonon spectra [13], or extracted from room temperature MD annealing runs.

@@ Finally, we expect our approach will prove optimal for refinements of large quasicrystal approximant structures, – several such "approximant" phases are known to exist in the AlNiCo system [14] – that are too complex to be handled by routine crystallographic refinement approaches.

Acknowledgments. We thank to W. Steurer for kindly providing us his experimental d-AlNiCo dataset, without which this work would not be possible.

References

[1] E. Abe, K. Saitoh, H. Takakura, A. P. Tsai, P. J. Steinhardt, H.-C. Jeong, Phys. Rev. Lett. 84 (4609) 2000.
W. Steurer, T. Haibach, B. Zhang, S. Kek, R. Lück, Acta Cryst. B 49 (1993) 661.

[2] B. Zhang, M. Estermann, W. Steurer, Z. Kristallogr. Suppl. 10 (1995) 120; S. Ritsch, C. Beeli, H. U. Nissen, T. Gödecke, M. Scheffer, R. Lück, Phil. Mag. Lett 74 (1996) 99; A. P. Tsai, A. Fujiwara, A. Inoue, T. Masumoto, Phil. Mag. Lett. 74 (1996) 223

[3] A. Cervellino, T. Haibach, W. Steurer, Acta Crystallogr. B 58 (2002) 8.

[4] H. Takakura, A. Yamamoto, A.-P. Tsai, Acta Crystallogr. A 57 (2001) 576.

[5] R. G. Hennig, E. H. Majzoub, A. E. Carlsson, K. F. Kelton, C. L. Henley, W. B. Yelon, S. Misture, G. Kresse, J. Hafner, Mater. Sci. A 294 (2000) 361; R. G. Hennig, K. F. Kelton, C. L. Henley preprint (cond-mat/020217) www.arxiv.org.

[6] M. Mihalkovič, I. Al-Lehyani, E. Cockayne, C. L. Henley, N. Moghadam, J. A. Moriarty, Y. Wang, M. Widom, Phys. Rev. B 65 (2002) 104205.

[7] C.L. Henley, M. Mihalkovič, M. Widom, J. Alloys. Compounds 342 (2002) 221.

[8] J. A. Moriarty, M. Widom, Phys. Rev. B 56 (1997) 7905; I. Al-Lehyani, M. Widom, Y. Wang, N. Moghadam, G. M. Stocks, J. A. Moriarty, Phys. Rev. B 64 (2001) 075109.

[9] M. Mihalkovič, W.-J. Zhu, C. L. Henley, M. Oxborrow, Phys. Rev. B 53 (1996) 9002.

[10] C. L. Henley, V. Elser, M. Mihalkovič, Z. Kristallogr. 215 (2000) 553.

[11] F .Gähler, S. Hocker, J. Non-Cryst. Solids (200x) this proceeding.

[12] Y. Yan, S. J. Pennycook, A. P. Tsai, Phys. Rev. Lett. 81 (5145) 1998

[13] M. Mihalkovič, H. Elhor, J.-B. Suck, Phys. Rev. B 63 (2001) 214301

[14] M. Doblinger, R. Wittmann, D. Gerthsen, B. Grushko, Mater. Sci. Eng A 294 (2000) 131.

orbit	object	x	b^{xy}	b^z	E_{site}
Al(1)	Node	0.075	3.34	0.34	0.04
Co(2)	Node^r	0.029	0.09	0.00	-2.21
Al(4)	Bond^r	0.104	0.92	2.79	-0.09
Al(5)	Fat	0.064	0.00	4.73	-0.22
Al(6)	Fat	0.128	2.15	2.45	0.24
Co(7)	Fat^r	0.064	0.31	0.05	-2.28
Al(8)	Fat^r	0.128	2.91	3.25	0.49
Al(9)	Fat^r	0.064	0.03	5.34	0.32
Al(10)	Boat	0.019	1.49	3.76	0.01
Al(11)	Boat	0.010	2.62	4.11	0.39
Al(12+)	Boat	0.010	0.00	0.21	0.65
Al(13)	Hex	0.030	1.23	3.63	-0.13
Al(14)	Hex	0.030	0.00	3.82	0.06
Al(16+)	Star	0.008	0.00	3.57	0.56
Ni(3a)	Node$_2$	0.079	1.05	0.40	-1.34
Ni(3b)	Node$_3$	0.049	0.24	0.24	-0.87
Ni(3c)	Node$_3$	0.025	0.92	0.36	-1.55
Ni(3d)	Node$_5$	0.055	1.24	0.50	-1.10
Al(15+)	Hex	0.015	0.82	5.37	0.61
Al(17)	Hex	0.015	2.22	4.83	0.82

Table 1. Atomic orbits in "augmented" binding. x is fractional content, b^{xy} and b^z refined anisotropic DW coefficients, and E_{site} are site energies in eV/atom, for the approximant T_{110}. Orbits above the horizontal line were unchanged from the "basic" binding. Superscript r denotes objects defined from the corners of the vertices inside the HBS tiles (Fat^r and Bond^r), see also Fig. 1

[15] M. Widom, I. Al-Lehyani, M. Mihalkovič, J. Non-Cryst. Solids (200x) this proceeding.

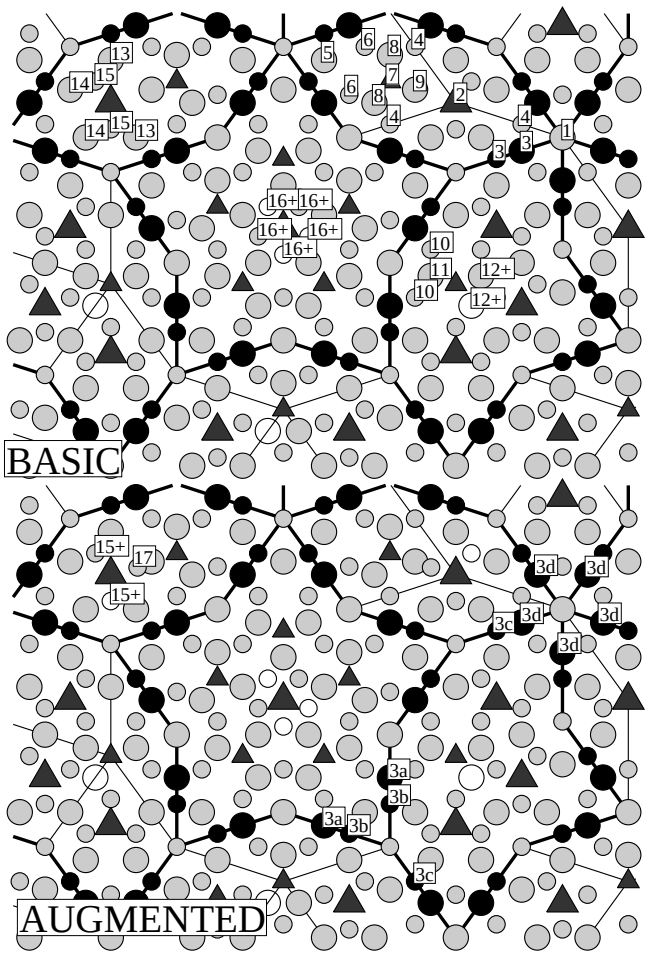

Fig. 1. Atomic decoration of the HBS tiling for "basic" (top panel) and "augmented" (bottom panel) bindings. Dark circles are Ni atoms, dark triangles Co, gray Al. Unoccupied sites are empty circles. Tiling orbits are shown as framed labels (once for each tiling object). Thick lines are HBS-tiling edges, thin lines edges of the inscribed rhombus tiling. For orbits that are binded to HBS tiles, the edges of rhombuses inside the tiles are not drawn. Each symbol occurs in two sizes, for upper and lower layer in the 4Å thick slice cut perpendicularly to the periodic direction.

binding	$N_{\rm obj}$	$N_{\rm orb}$	$N_{\rm pos}$	$N_{\rm par}$	$E_{\rm rel}$
basic	9	16	38	72	-0.400
augmented	13	23	58	106	-0.395

model	b_{perp}	R_w	R	E
T_{42}-basic	3.65	0.122	0.202	-0.372
T_{42}-augmented	4.15	0.089	0.169	-0.344
T_{110}-augmented	3.88	0.082	0.152	-0.330
(smaller λ)	3.93	0.086	0.159	-0.370

Table 2. *Top:* Numbers of tiling objects $N_{\rm obj}$, orbits $N_{\rm orb}$, positional parameters $N_{\rm pos}$ and total number of fit parameters $N_{\rm par}$ (including anisotropic DW factors and the global $b_\perp$ DW factor). The last column is the energy per atom after constrained relaxation, without use of diffraction data. *Bottom:* summary of the results for the combined fits, giving the perp-space Debye-Waller coefficient, the weighted (R_w) and unweighted R factors. The last row reports an alternative refinement result for approximant T_{110} with the "augmented" decoration rule, in which the λ parameter in Eq. 8 was kept smaller to achieve lower energy.

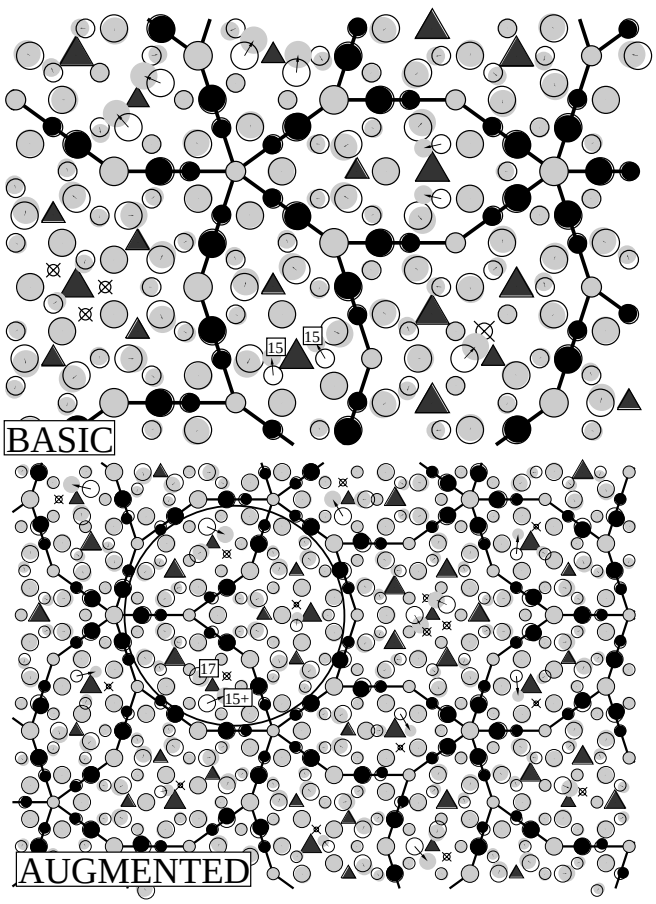

Fig. 2. *Top:* "basic" decoration rule, refined model. Arrows indicate displacements (empty symbols stay at the "ideal" starting position) that occured during combined fit. Vacant sites are shown as small circles and marked by crosses. *Bottom:* "augmented" binding, refined model. One decagonal columnar cluster is marked by two dashed circles, near the outer shell of atoms, and near the inner ring of 10 TM atoms.

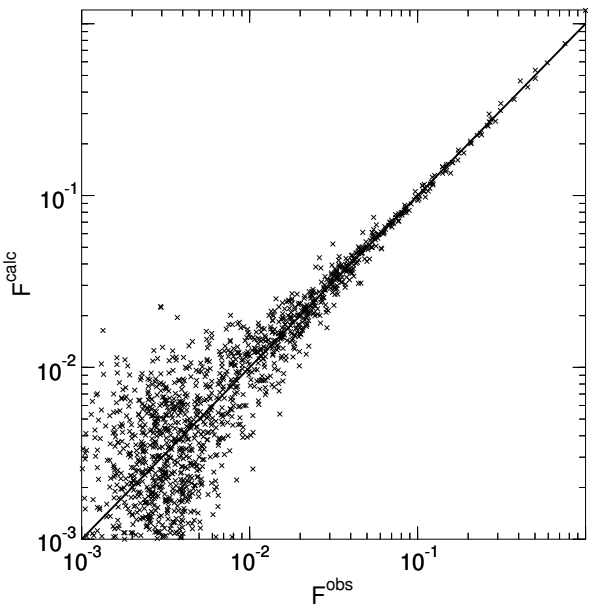

Fig. 3. Observed vs calculated diffraction amplitudes for approximant T_{110}, final refined model of the "augmented" binding.